Contents

Chapter 1

Electric characterization

1.1 Electric scheme and description

In this chapter is discussed the development of Plasma Coagulation Controller eletcric scheme and its characterization. Circuit design, as the entire model design, is highly influenced by needs of flexibility and mobility of the source for wound treatment. To produce plasma as DBD, in air, with helium or argon as ignition gasses, it is necessary to apply high electric fields in little space. Manwhile, to make possible easy medical application the source head (where there si plasma output) must be compact, with particular attention to electric safety measuraments. It is common to produce electric fields with fast voltage pulses for various uses, including jet or DBD plasma production ([35], [16], [10])), the scheme used in this study outputs a voltage pulse with an amplitude from 1 kV to 10 kV and pulses frequencies from 5 kHz to 60 kHz.

A rappresentation of power and signal lines is in figure 1.1. The circuit is divided mainly in two parts : the controller, with alimentation and settings controls, and the head, where the discharge happens and plasma is emitted.

Lines divides in:

- **Alimentation** : the 220 V DC power line goes in a transformer that gives a reduced tension to the head, 22 V in the figure, passing through a diode bridge. This tension aliments the Driver Circuit on the head.

- **Arduino and trigger** : the power line is reduced to 12 V necessaries to aliment an Arduino controller and a laser. From an Arduino analogical output a PWM wave goes to the laser trigger, it transmits information on the wave, frequency and duration, with an optical fiber that ends with a photodiode installed on the driver circuit. Wave frequency is setted by the Arduino, wave duration is setted giving the opening time of the MOSFET that passes the signal to be amplified and sent to the head's transformer. With this setup the high-voltage line is entirely decopuled from the controller, so there are not problems of signal reflection on the power line or the Arduino.

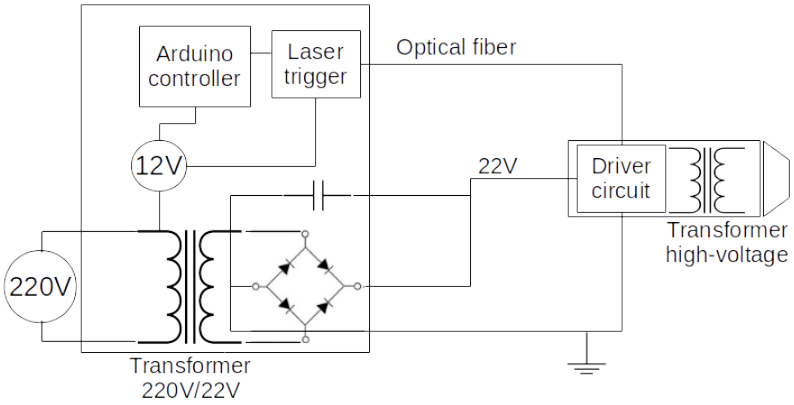

Figure 1.1: Scheme of the general electric line to produce high voltage, the controller on the left and the head on the right.

- **Head** : the Driver Circuit receives a power line and an optical trigger that defines frequency and duration of the voltage pulse. When the trigger gives the start signal, the transformer on the head receives on primary circuit a voltage of hundreds V and outputs from secondary circuit a voltage of thousends V. Connected to the output there is the electrode inside a capillary tube of dielectric material.

To understand signal propagation is presented a simulation in figure 1.2, obtained with a simplified scheme with Spice. As shown, once the PWM trigger starts, tension on the primary goes from alimentation value to 0, when the PWM signal ends (after 6 µs, it has a pulse with amplitude of 150 V (width of 1.2 µs) and a pulse of −5000 V at the output of secondary circuit. A longer PWM implies a longer charging time, so an higher pulse. Ultimately, amplitude of the pulse is proportional to the width of the PWM signal and to know working conditions of the source it is necessary to study relation between opening time and amplitude output on the actual circuit.

During this thesis study were built two sources, with two controllers and heads, the first one will be called source A, the second one source B. From an electrical perspective the two models are almost identical, the second one comes with a low-pass filter on the driver circuit (to diminish high frequencies noise) and higher amplitude capabilities thanks to a different turns ratio in head's transformer. The characterization of electric features is made measuring output tension and current with different settings.

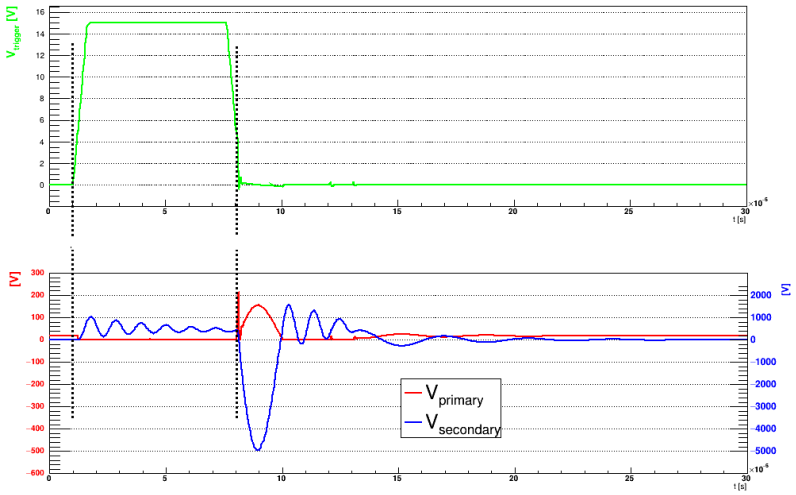

Figure 1.2: Scheme of signal propagation. Up, in green, there is the optical trigger, down, in red, the voltage of primary circuit in the head with axis on the left, in blue, the voltage of secondary circuit with axis on right.

1.2 Output characterization

Plasma ignition and discharge features are regolated by electric field generated in the circuit head and power deposition to flowing gas, so the parameters involved are pulse amplitude and frequency arriving on the electrode, settable in the circuit. Medical application of plasma requires low current intensity, in this study it's measured current intensity flowing on a copper sheet targeted by the plasma plume at a certain distance. Ultimately the different parameters for the measures are: Δt, opening time of the trigger that defines amplitude of the pulses, and f, frequency of the pulses.

Voltage signals are taken with an high-voltage probe *Tektronix P6015A*, attenuation $\times 1000$, current signal with a *Tektronix CT2* probe that gives a 1 mV for a current of 1 mA. All signals are measured with a *Yokogawa DL9040* oscilloscope, from which is saved the waveform of voltage and current.

Measures are taken without gas flowing, to see clean output voltage of the circuit, and with an helium flow of 2 L/min, to measure the actual output in presence of plasma, with different amplitude and frequencies. It's also measured an effective current intensity, i.e. a mean value in a time period, to evaluate plasma application's effects on biological tissues.

Every lenght measure is done with a decimal caliper, it's taken an uncertainity of 0.1 mm.

1.2.1 Measures without gas

It's used the hv probe to pick tension's differences between secondary circuit ouput and ground. Once a work frequency, f, is set, we take voltage wave shape for different values

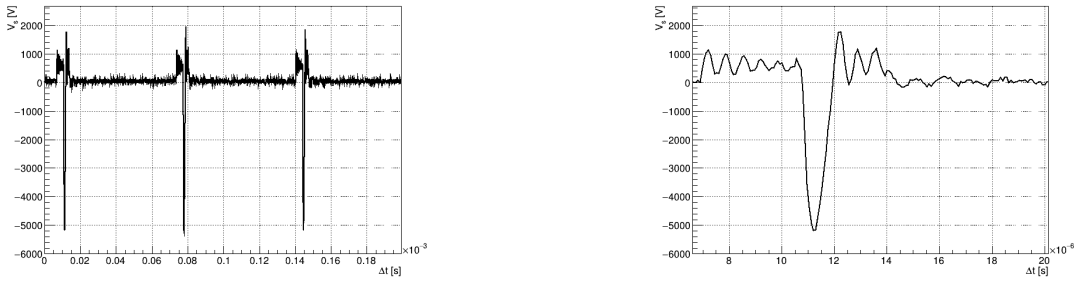

(a) Three pulses **(b)** Zoom on one pulse

Figure 1.3: Example pulses with source B for $f = 10\,\text{kHz}$ and $\Delta t = 2\,\mu\text{s}$

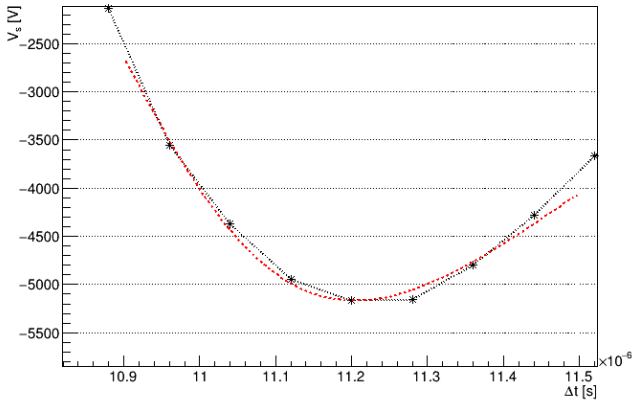

Figure 1.4: Example fit with source B for $f = 10\,\text{kHz}$ and $\Delta t = 2\,\mu\text{s}$

of opening time of the circuit, Δt, in the selectable range. To assure that a voltage pulse ends before another starts, this range is different for different frequencies: higher work frequencies means more pulses in a given time, taking into consideration pulse oscillations, the range of possible Δt is smaller at higher frequencies. A typical measure is shown in figure 1.3.

The main pourpous of the measures is to study proportionality between amplitude of the peak and opening time, for different frequencies. Those signals are analyzed evaluating their Fourier Transform (using ROOT C++ libraries [30]) and reconstructing the signal without higher frequencies, to exclude noise fluctuations. The reconstructed peak is an asymmetric function in time as in figure 1.4, it's possible to interpolate it with a Landau function [7] and obtain peak value and position. The error from the fit function is added quadratically to the error given by the cut of high Fourier frequencies, evaluated as the square root of the mean square difference between reconstructed and original signal for every point included in fit range.

Results are shown in figure 1.5 for the two sources. In source A we can see a linear

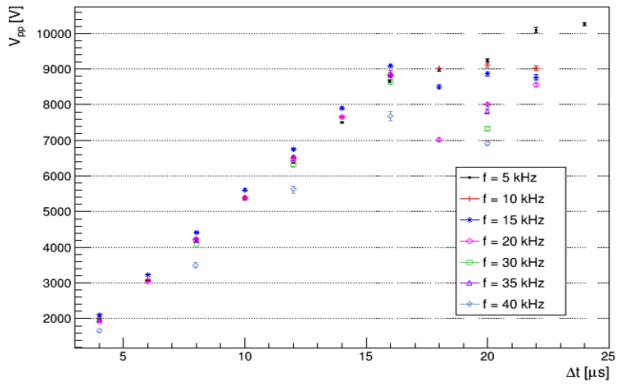

(a) Source A

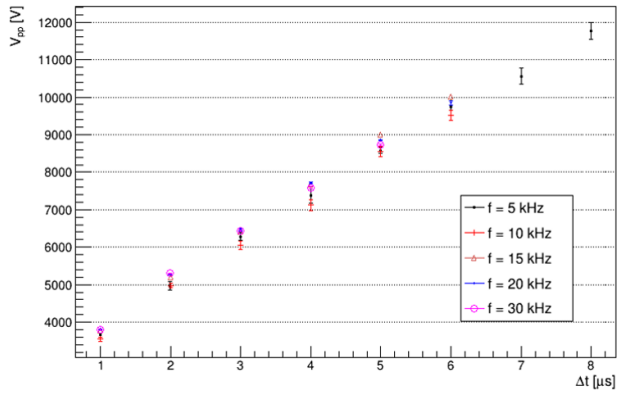

(b) Source B

Figure 1.5: Absolute peak's value of secondary circuit in function of Δt at different f, for both sources.

behavior for $4 \leq \Delta t \leq 16\,\mu s$, with tensions from 2.02 ± 0.01 to $9.25 \pm 0.05\,kV$; for greater Δt data loses linearity. The upper limit on chosen Δt is given by the need of a minimum time interval between two pulses. Also in source B we can see a linear behavior, but tension values are larger, for $1 \leq \Delta t \leq 8\,\mu s$ tension goes from 3.66 ± 0.06 to $11.76 \pm 0.22\,kV$. With this source the upper limit for Δt is chosen observing voltage output: measures are taken only for tensions needed to have plasma in a DBD regimen, higher opening times would only stress more circuit components. Both sources have near the same output for different frequencies, to confirm it datas are fitted with a linear function in the range $0-16\,\mu s$ for source A and range $0-8\,\mu s$ for source B. Evalueted parameters are compared, as shown in figure 1.6. The values are displaced with random distances from the mean value, so it can be concluded that the behavior is not defined by the frequency.

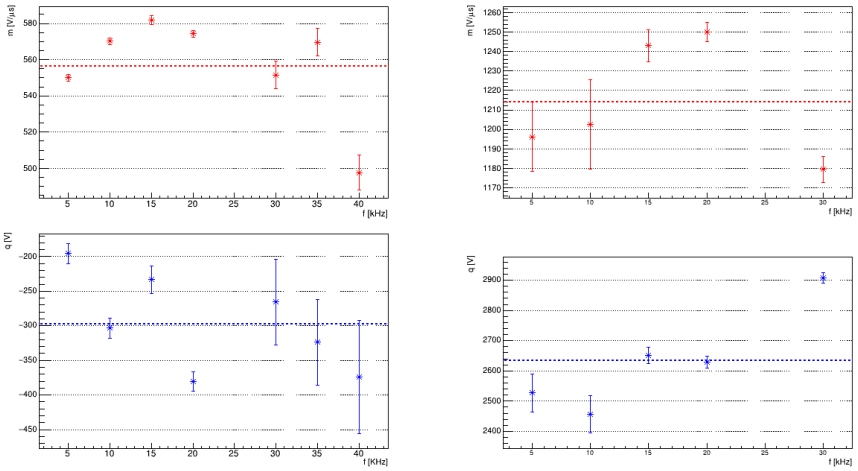

(a) Source A **(b)** Source B

Figure 1.6: Voltage peaks are fitted with a linear function $V_{peak} = m\Delta t + q$, in figure we see fit parameters at different frequencies for both sources, in dashes the mean value.

1.2.2 Measures with gas

Introduction of an helium flow at the end of the head will produce plasma ignition, tension will be different, and it will be possible to measure current intensity carried by plasma. To assure safety of plasma application, that cells aren't damaged by plasma, it must be avoided a large current intensity and arc formation. Studies of conditions for DBD discharges and arc transitions ([19], [32], [33]) suggests that for fast pulses it's safe to have current intensity $< 10\,\text{mA}$.

Current intensity is measured using a copper sheet with dimensions $10\,\text{mm} \times 10\,\text{mm} \times 1\,\text{mm}$. Plasma plume impacts on the sheet, the current probe is connected to it and sends a voltage signal to the oscilloscope, with cable shielding to lessen interferences. Current intensity and target distance relation is studied in[28], in this study the distance between target and electrode is chosen around typical value for treatments permitted by head's sources geometry: $10\,\text{mm}$ for source A and $15\,\text{mm}$ for source B (a bit longer due to electrode position in the head).

In figure 1.7 can be seen a typical measure for $\Delta t = 8\,\mu\text{s}$ and $f = 5\,\text{kHz}$ with source B. For both sources there is a current peak in correspondence of voltage pulse that increases with tension, however for source B there are measures where the peak is so low that it is covered by noise.

Data analysis is done as before, cleaning measures from noise, estimating the peak and it's error. Results are shown in figures 1.8 and 1.9, measures where the current peak is not distinguishable are excluded from plots.

Tension peaks are slightly lower then values without gas, as expected seeing the plume as an additional load at the end of the circuit ([23]), but the linear behavior for

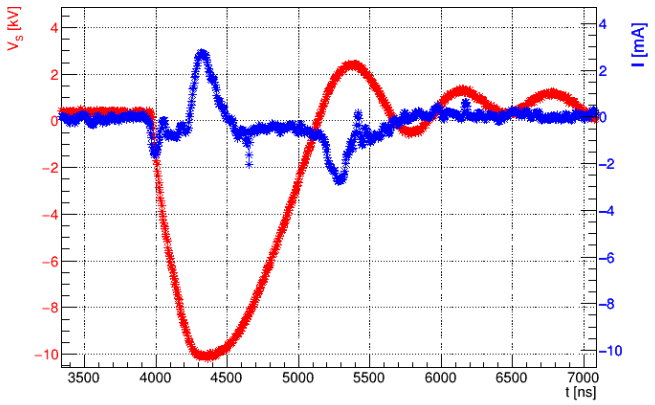

Figure 1.7: Example measure with source B for $f = 5\,\text{kHz}$ and $\Delta t = 8\,\mu\text{s}$

$V_{pp} \leq 10\,\text{kV}$ remains and we can compare linearity for different frequencies. Current intensities grows with tension and are higher for source A, as expected given different distances electrode-target. Analysis of linearity also for those measures can show if there is a different behavior changing pulse frequency or source. Figures 1.10 and 1.11 shows results of the linearity study at different frequencies. Tension values, for both sources, are scattered around the mean value parameter without a clear behavior, confirming independence hypotesis of voltage growth from pulses frequencies. For source A we find a slope parameter $m_V = 0.366 \pm 0.001\,\text{kV}/\mu\text{s}$, for source B $m_V = 1.145 \pm 0.008\,\text{kV}/\mu\text{s}$, larger due to the different circuit, as mentioned before. Current values shows a different behavior: in source A we find a stady increase of parameters with higher frequencies, in source B data are more scattered and we couldn't extrapolate a behavior. However current slope is in the same range of values for the sources, with a maximum for source A of $m_I = 1.10 \pm 0.01\,\text{mA}/\mu\text{s}$ and for source B of $m_I = 1.04 \pm 0.17\,\text{mA}/\mu\text{s}$. An explanation for parameter's trend in source A it's that for higher frequencies the interval between two pulses it's smaller and oscillations of electrode potential after a pulse influences more gas ionized fraction, so mean density value of charged particles is higher for higher frequencies. Due to low signal to noise ratio in measures for source B, it is not possible to esclude a relation between current slope (how much current intensity grows increasing opening time) and pulse frequency, however it is established a maximum limit value to take into consideration when using the device.

1.2.3 Plasma impedance

From tension and current measuraments we can define plasma's electric behavior, in this subsection source B measures are used to estimate plasma impedance. Tension output from head's transformer can be modelized as a dumped sine wave around the peak, as in equation 1.1.

$$V_S = V_0 + V_{\text{pulse}} \sin\left(2\pi f_{V_s} t\right) e^{-t/\tau} \tag{1.1}$$

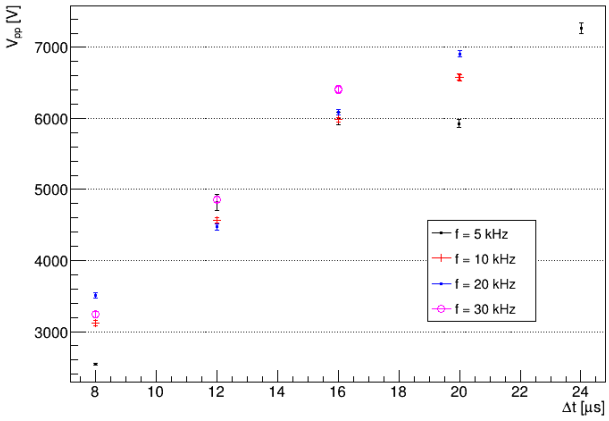

(a) Source A

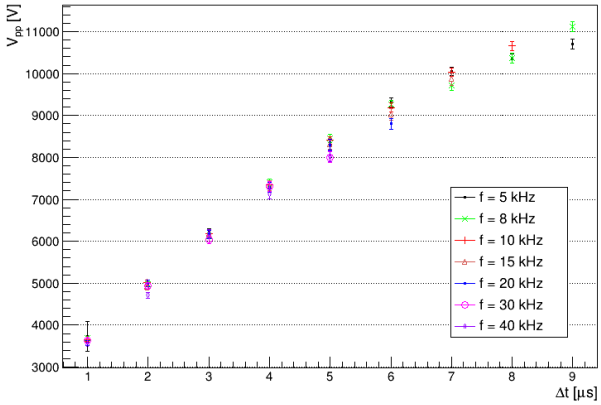

(b) Source B

Figure 1.8: Absolute peak's values of secondary circuit output in function of Δt at different f, with an helium flux of 2 L/min, for both sources.

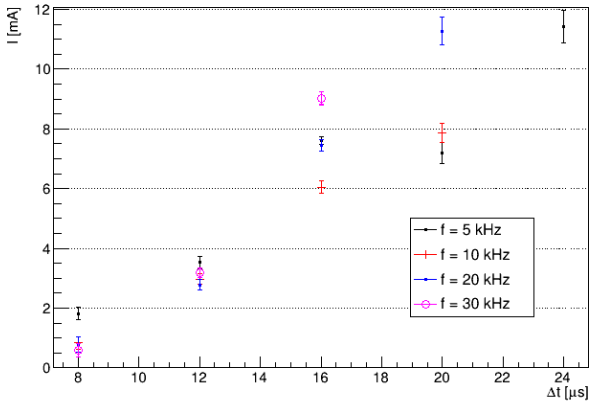

(a) Source A

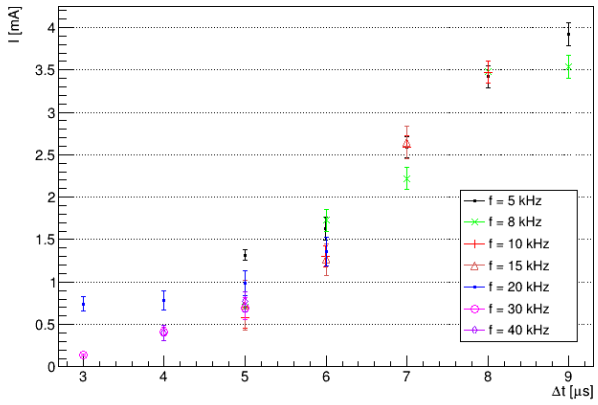

(b) Source B

Figure 1.9: Absolute peak's value of current intensity on copper target with an helium flux of 2 L/min, in function of Δt at different f, for both sources.

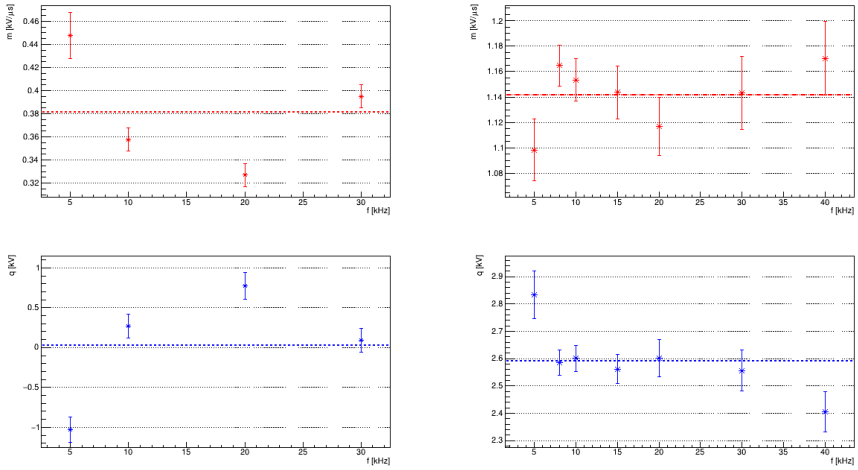

(a) Source A **(b)** Source B

Figure 1.10: Voltage peaks are fitted with a linear function $V_{peak} = m\Delta t + q$, in figure we see fit parameters at different frequencies for both sources, in dashes the mean value.

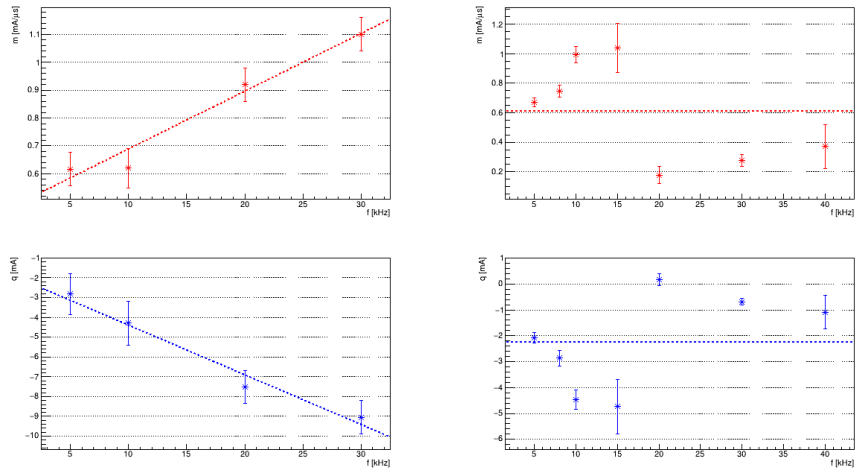

(a) Source A **(b)** Source B

Figure 1.11: Current peaks are fitted with a linear function $I_{peak} = m\Delta t + q$, in figure we see fit parameters at different frequencies for both sources. For source A we see in dashes a linear fit, for source B the mean value.

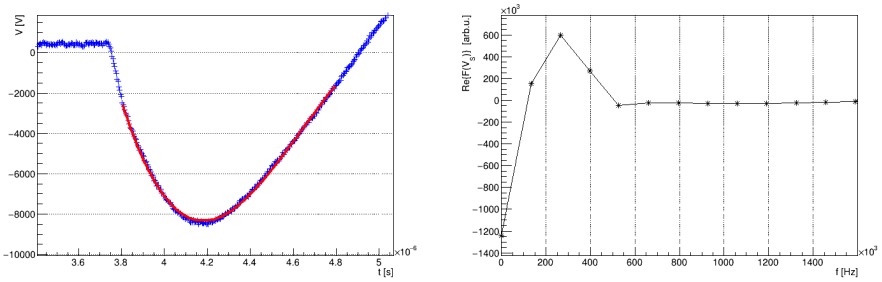

(a) Dumped sin fit **(b)** Fourier transform

Figure 1.12: On the left example fit of a tension peak, $f = 8\,\text{kHz}$ $\Delta t = 5\,\mu\text{s}$ with function 1.1; on the right the fourier transform of the measure in the interval $[3 - 6\,\mu\text{s}]$ that shows the frequency peak f_{V_s}

This formula gives an explicit parametrization for f_{V_s} that is an estimation of the frequency of the single pulse (the frequency that defines rise and fall of the pulse, different from the work frequency of different pulses imposed by Arduino, called f). This parameter is important because plasma's electric behavior depends on this frequency, analyzing signal with different frequencies f_{V_s} it's possible to understand plasma's parameters. Frequency pulse it's different for every opening time of the circuit, Δt, but it's constant when changing frequency of pulses, as explained before analyzing tension outputs at different frequencies. In figure 1.12 are presented examples of a peak fitted with the function in formula 1.1 and it's fourier transform to show peak frequency corresponding to f_{V_s} for that specific Δt. In figure 1.13 are shown different resulting parameters for different Δt.

Fit parameters follows always those presented: as expected, with higher opening times V_{pulse} grows while f_{V_s} and τ have their own behaviors that depends from tension secondary output V_s. To estimate plasma's impedance it's useful to observe that voltage peak is quite large in time: it varies of less then 3% of peak's value in an interval of 150 ns around it. As tension and current peaks times differs always by a time interval $|t_{V_p} - t_{I_p}| \leq 150\,\text{ns}$, it's possible to assume $V_{t_{I_p}} \simeq V(t_{V_p})$, i.e. that tension during the current peak maximum is equal to tension's peak value. With this approximation, it makes sense to plot tension's peak values against current's peak values, as in figure 1.14, and given a Δt it's possible to give an estimation of impedance module as $Z = \frac{V_p}{I_p}$. Resulting impedance are shown in figure 1.15, changing opening times and changing frequency of single pulse f_{V_s}.

From the graphs it's possible to extrapolate that plasma impedance goes from $2.98 \pm 0.11\,\text{M}\Omega$ to $11.82 \pm 2.19\,\text{M}\Omega$, with near constant values in the range of opening times $7-9\,\mu\text{s}$. From a deeper analysis and specific measures it could be possible to expand the analysis here presented and estimate plasma's electrical resistance, capacitance or induttance.

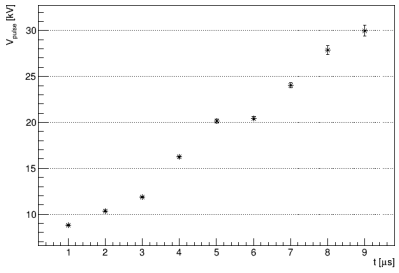

(a) V_{pulse}

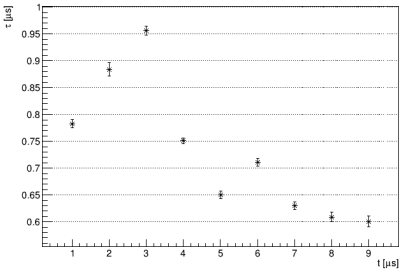

(b) τ

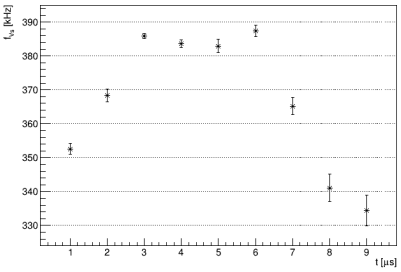

(c) f_{V_s}

Figure 1.13: Fit parameters of pulses with $f = 8\,\text{kHz}$ for different Δt.

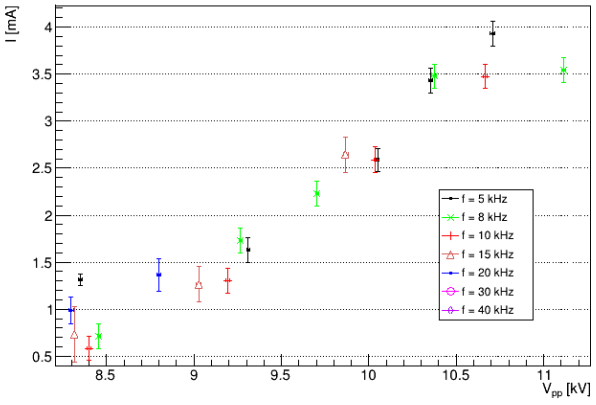

Figure 1.14: Tension's peak values against current's peak values for different Δt and frequencies.

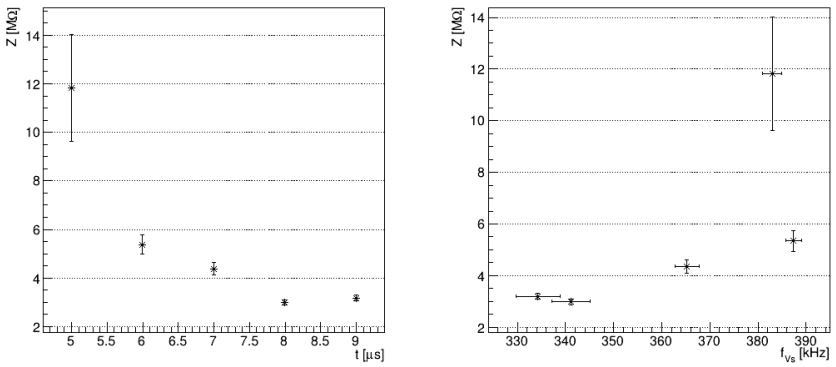

Figure 1.15: Impedance module estimation for different opening times (left) corresponding to different frequencies (right).

1.2.4 Effective current

Current effects in applications on biological tissues have to take into consideration current intensity in a time interval tipically larger then the pulse widths used in our sources ([34], [28]). It's possible to estimate an effective current that is more appropriate to take into consideration when evaluating damage due to currents, as a mean of current intensity in a defined time interval calculated with equation 1.2, taking $t_2 - t_1 = 1\,\text{ms}$. The effective current takes into consideration that current values are very small for all the time between two pulses.

$$I_{\text{eff}} = \frac{1}{(t_2 - t_1)} \sqrt{\int_{t_1}^{t_2} I^2 \, dt} \tag{1.2}$$

Figure 1.16 shows effective currents measured for both sources. Values are significantly smaller then maximum peak values, expecially for source B where oscillations after the main peak are smaller. The maximum value for the two sources is given by $I_{\text{eff}A} = 2.47 \pm 0.07\,\text{mA}$ and $I_{\text{eff}B} = 0.23 \pm 0.01\,\text{mA}$.

1.2.5 Time intervals

Time width of signal affects reaction's probabilities (chapter **??**) and plasma's power deposition(chapter **??**), here we try to give an estimate of those time intervals. It can be defined as the FWHM of measured peaks, evaluated as the time when we measure half of tension or current maximum value. As the characterization of the sources shows an almost equal behavior, this study is made only for the latest version of the source, that's the only one used in the following chapters. Results are shown in figure 2.5. For every frequence there is a quadratic behavior of tension widths with a minimum for a $\Delta t = 5\,\mu\text{s}$ that depends on circuit scheme. It is possible to give an estimation of pulse width with a mean value between this minimum and maximum values obtained for $\Delta t = 1\,\mu\text{s}$, it is

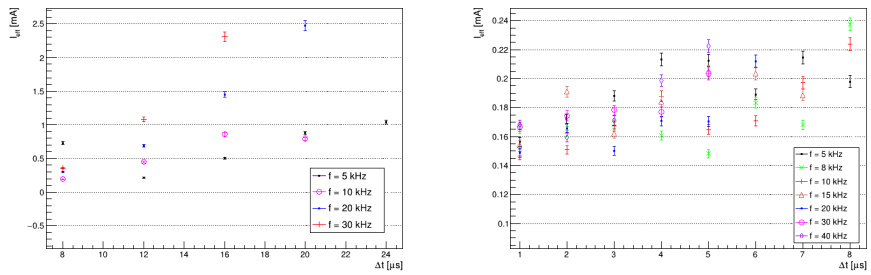

(a) Source A **(b)** Source B

Figure 1.16: Effective currents in a time interval of 1 ms.

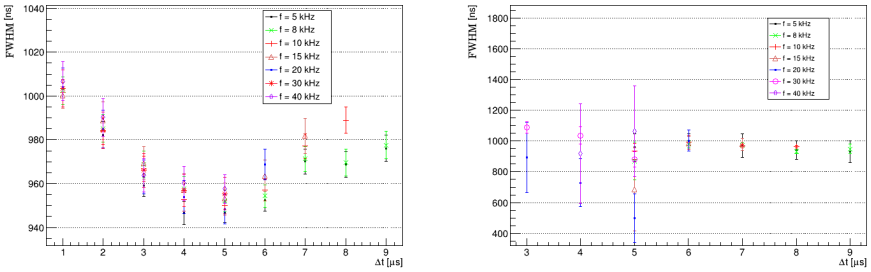

(a) Voltage **(b)** Current

Figure 1.17: FWHM of tension and current peaks varying opening time, for different frequencies.

$T_V = 963 \pm 15$ ns. For currents, widths have great uncertainity where the peak is low, but it is possible to evaluate a mean value for $\Delta t \geq 6\,\mu$s, and it is $T_I = 968 \pm 28$ ns. Values from the two measures are compatible and they are a good estimation of pulse time duration.

Chapter 2

Shape and dynamics

When it's seen by the eye, plasma sources for medical use expels a little plume of plasma that emits radiation in a visible range, with different colours or intensity that depends on the gas composition, it's flow and intensity of applied electric field. However if we see the plasma at a specific time, recent studies shows that what is expelled is not a continuos flow of plasma, but the plume is formed by compact bullets with high velocities ([24], [29]). An example of this phenomenon is shown in figure 2.1, measured with the experimental apparatus explained later.

Plasma bullets still needs to be studied in depth, we only know their basic dynamic of formation and expulsion. Some general features are that:

- bullet's velocities are $> 10\,\mathrm{km/s}$;
- bullet formation, it's velocity and it's travel distance depend on applied tension on the electrode;
- frontal image of the bullet, on a plane perpendicular to it's velocity, is not a full circle but it's donut shaped, with an outer ring of higher intensity.

The scope of this experiment is to observe plasma bullets produced with our source, their shape and their velocity and how they change with different discharge conditions.

Given their typical velocities and the temperature of the plasma, bullet propagation is tought to be related to a travelling ionization front. This propagation can be studied with simplified simulation of DBD discharges, where it's reproduced the behavior of plasma bullets ([37], [5]) or the interaction between plasma and a target ([27]).

2.1 Experimental setup

The scope is to visually observe dynamics of plasma formation and propagation, so it's needed an acquisition setup with an high-speed camera (little integration time), around 10 ns, and an image intensifier that permits to visualize light emitted in such a short time interval.

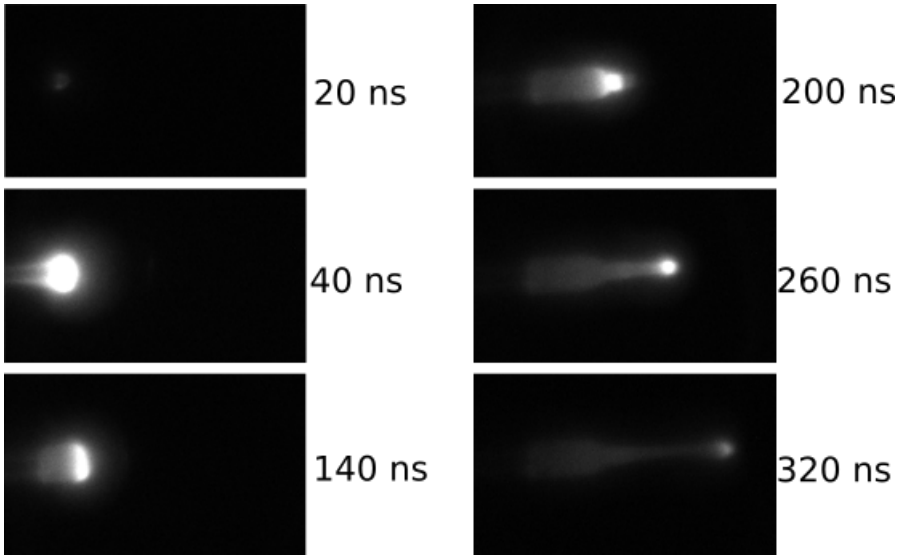

Figure 2.1: Example of plasma bullet expulsion, as measured with our experimental setup.

This is a measure where we need coincidence between discharge and frame measure so it is necessary to consider instruments and plasma source specific delays and give appropriate triggers.

Experimental setup is shown in photo 2.2 and a scheme is presented in 2.3, there are the trigger signal lines, optical acquisition pointed at source exit and measure acquisition composed by a computer and an oscilloscope.

2.1.1 Source and optical setup

Source head is positioned vertically and emitted light is collected from the side. Optical apparatus is composed by a lens coupled with a Micro Channel Plate image intensifier (MCP). An MCP works as in figure 2.4: for every photon received, thanks to an high-voltage power supply, it emits many photons.

Those photons are received by an high-speed camera *Point Grey Flea* ([1]) equipped with a CCD of 1024×768 square pixels $4.75\,\mu m$ wide. Every frame is sent to the pc where FLIR software elaborates and saves them in pgm format ([2]).

2.1.2 Source, power lines and electric signals

It's used a source with electric features and functioning similar to those described before, with an output between 3 and 8 kV, variabile changing Δt of the trigger signal (see 1), that is always given through an optical fiber with frequency f. Differances are that tension is positive and not negative, because it helps formation of the plume with gasses harder to ignite (e.g. Argon), and that trigger signal is given by a generator function (2 in the scheme) to define discharge time respect to the trigger of other instruments.

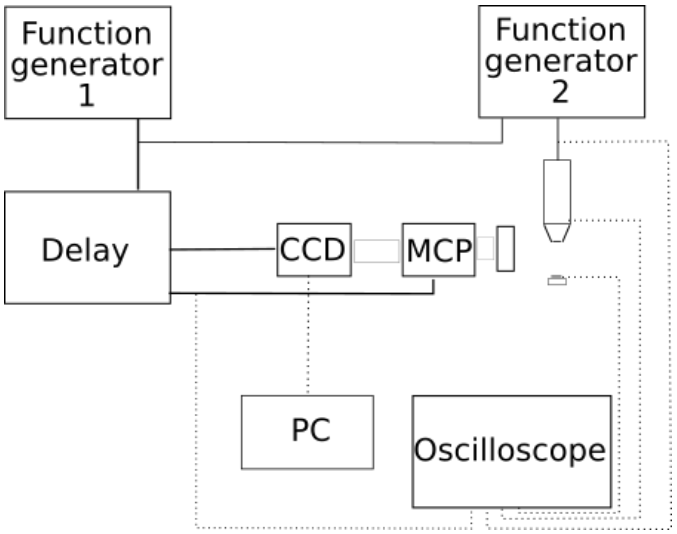

Figure 2.2: Photo of the experimental setup.

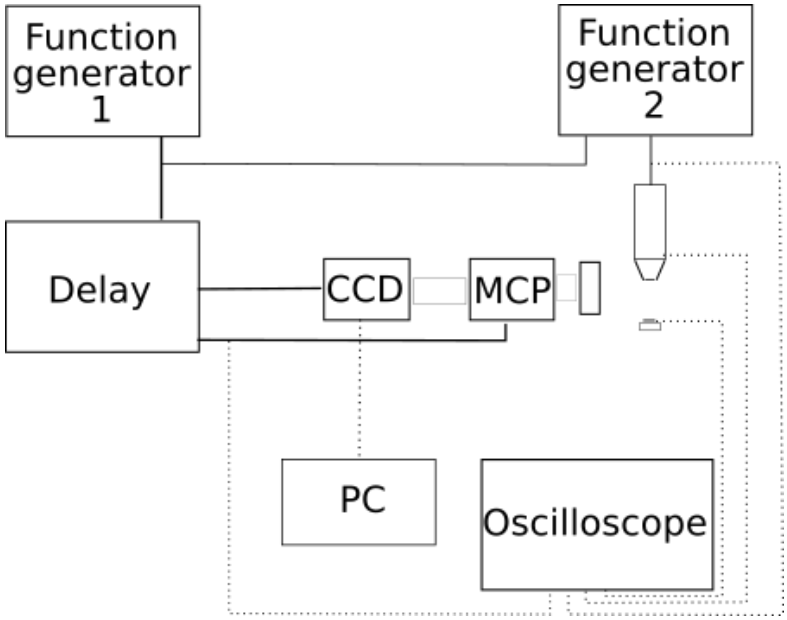

Figure 2.3: Experimental setup scheme. Function generator 1, function generator 2 and delay generator send trigger signal to camera (CCD), to source and to image intensifier (MCP), full lines in the scheme. Camera sends measured frame to a computer (PC) and from source, source's target, function generator 2 and delay are taken signals read on the oscilloscope, pointed lines in the scheme.

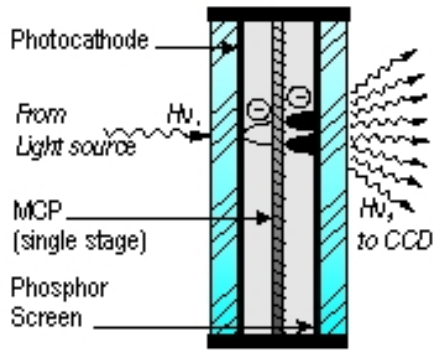

Figure 2.4: Micro Channel Plate image intensifier functioning.

The source is positioned vertically at a distance of 42.0 ± 0.1 mm from optical bench, with the glass nozzle that permits to observe plasma formation inside it (external diameter 8.0 ± 0.1 mm, internal diameter 6.0 ± 0.1 mm), with a distance from the end of the electrode to nozzle exit of 12 mm.

Under the source is possible to put targets where plasma impact, are used two different targets at different heights: conductive target and insulator target. The first one is a copper square sheet of dimensions $10\,\text{mm} \times 10\,\text{mm} \times 1\,\text{mm}$ (used for current measures in chapter 1), the second one is a simple plastic material.

CCD camera is powered by the connection to acquisition computer while image intensifier MCP is powered by an high-voltage supply, both are triggered by the delay generator, with different times (see next section).

On an oscilloscope are measured the trigger signal given to source head, the trigger signal given to MPC, the voltage electrode with high-voltage probe *Tektronix P6015A* and the current intensity when it's used the conductive target. Current intensity measure is done measuring voltage drop on a resistance of $1\,\text{M}\Omega$ with a probe $x10$.

2.1.3 Trigger synchronization

Experiment's scope is to know plasma dynamics at a specific point on voltage waveform, so it's necessary to know precisely discharge and measure times.

To compose the necessary trigger line are utilized:

- function generator *Or-x 310*, 1 in figure, that sends a square wave with set amplitude, width and frequency f;
- function generator *Lecroy 9210*, 2 in figure, that sends a square wave with frequency given by the trigger, amplitude set, and variable width Δt;
- delay time generator *Stanford DG535*, that sends square wave with set amplitude, frequency given by the voltage input and starting times given by voltage input startin time plus settable delays (4 channels).

Every intrument has it's own time that elapse between trigger signal and effective measure. The longer one is arming time for high-speed camera in the order of ms, the tinyest one is integration time for acquisition system, that starts from the activation of the image intensifier and span 15 ns.

A time line is shown in figure 2.5, an example of signal taken with the oscilloscope is in figure 2.6. There are three relevant times defined by function and delay generators:

1. t_0 is the starting time for the square wave given by *Function generator 1*, with an amplitude of 5 V and a frequency f, that goes as external trigger to *Function generator 2* and as voltage input to *Delay generator*. From *Function generator 2*, at t_0, starts the square wave that triggers discharge and arming of camera, for a time given by Δt that will define voltage amplitude (see chapter 1) and the same trigger frequency f. From *Delay generator*, at t_0, without delays, starts the trigger signal to arm the camera with the CCD.

2. t_{DIS} is the effective discharge time, when the amplitude peak starts. From trigger signal end to amplitude peak start there is a time delay given mainly by the response time of photodiode. Measuring the signals as in figure 2.6, it's possible to estimate this delay as 987.7 ± 56.7 ns, constant for every f and Δt. Once the discharge starts, in the grey zone in figure, there are the events that we want to measure, plasma formation and propagation.

3. t_{MIS} is the measure time, when the MCP is triggered on. The delay between t_0 and t_{MIS}, t_D, is given by the *Delay generator* with possible steps of 1 ps. Changing t_D during measure it's possible to see plasma dynamics at different times that corresponds to different points on electrode tension waveform, as in figure 2.6.

Integration time for a single frame is 15 ns, so the time step between two measures has to be larger then it. For slow plasma bullets (Neon or Argon) it's used a step of 50 ns, for fast bullets (Helium) it's used a step of 20 ns.

The effective measure time have to consider slower time of the camera, larger then 50 ms. It's important to note that also with little frequencies, around 50 Hz (see later the minimum working frequency for different gasses), time between two pulses is 20 ms, so it is not possible to see two consecutive frames, we observe the same time in different discharges.

Changing the settings on camera acquisition software is possible to measure a signal below pixel's saturation point. One of the parameters is the *Shutter time*, the opening time of the camera shutter, that if set on a value larger then the time between two signals permits to integrate between two frames. When we work with a gas, we select an appropriate *Gain* value and an appropriate *Shutter time*, chosing to work measuring a single discharge frame or a multiple discharge frame.

2.1.4 Different setups

Plasma formation is influenced by many parameters such as frequency of high-voltage pulses, their rise time and maximum, gas type, gas flow, presence of a target and its

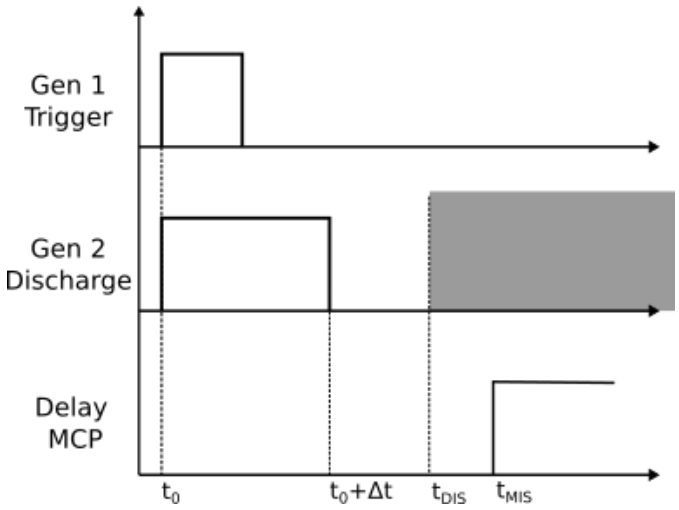

Figure 2.5: Time signal synchronization scheme: t_0 is the starting trigger time, Δt is the opening time for plasma source (see chapter 1), t_{DIS} is the starting time for the discharge and t_{MIS} the starting time for the MCP i.e. the measure time

.

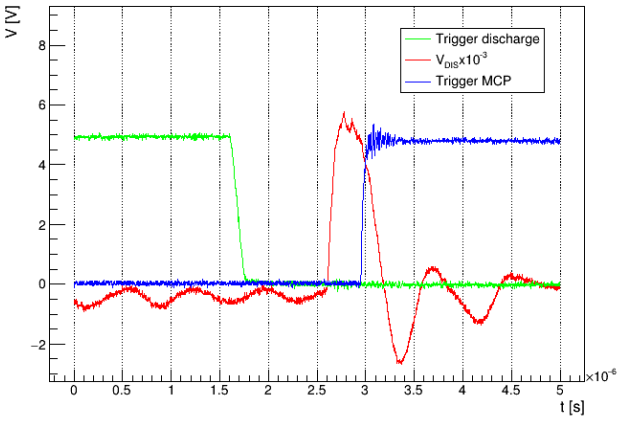

Figure 2.6: Oscilloscope measure example, in green the discharge trigger, in red the electrode tension output and in blue the MCP trigger.

features (see [24], [17]).

For pulse frequency we find a lower limit value, different for each ignition gas, under which there is no discharge. For frequencies higher then this value we don't expect changes (as there aren't in the electric behavior in chapter 1), so we use a single chosen value that permits plasma ignition and doesn't stress the experimental setup. High-voltage values and gas type determine plasma bullet formation and affect its expulsion velocity. In particular, different gasses have different atomic mass and ionization energies, they will have different voltage ignition values and reactive species formed in plasma will have different velocities. Gas flow influences how much gas there is when the ignition starts, so varying it we observe different bullets diameter and velocity. Target influences bullet expulsion, propagation and plasma rebound signal. With a conductive target near plasma exit we will have an easier path seen by charges that propagates and, once the bullet hits the target, its observed higher luminosity going from the target to the electrode. With an insulator target we don't find the ionization channel closing on the target, but we observe charge deposition on the insulator with a shape that depends from the gas and the target. In some setups, to help plasma ignition it's also used a conductor ring at ground potential or at floating potential, placed around source nozzle, after the electrode position.

In this study we present different setups with three different gasses, as shown in table 2.1.

2.1.5 Frame analysis and calibration

Once a measure setup is chosen, t_D is set around the start of the discharge, we measure the oscilloscope waveform for every channel (setup as explained before), and from them we save 5 frames for every t_D varying it with steps of Δt_D. Measures are taken until the end of the main tension peaks and the camera doesn't see anything.

From oscilloscope waveforms we can extrapolate the measure time from the start of the discharge and tension value at measure time. When there is the conductive target it's also possible to see current intensity and it's peak time.

Frame analysis is done converting the pgm files in 2-dimensional histograms, using *TH2* class written in *ROOT* libraries (see [8]). We are interested in plasma bullet formation and it's expulsion, but also in other fenomenological behavior that is observed during measures. For plasma bullet we take the mean for every pixel between the five frames taken, from then it's isolated the plasma bullet as the collection of pixels with maximum intensity in considered zone. From this image we can extrapolate the center of the plasma bullet, it's velocity and it's x and y diameter.

Relative dimension of what we are observing is found with a calibration with a given target. It's used a plate with 4 holes, with diameter of 1.00 ± 0.05 mm at the vertice of a square with an edge lenght of 10.00 ± 0.05 mm, positioned where there is pasma during experiments and illuminated from behind. Acquiring a frame of this setup it's possible to extrapolate pixel distances that corresponds to 10 mm for every square edge, average them, and calculate pixel's width in our frames, resulting a value of $d_{pix} = 0.172 \pm 0.002$ mm.

Gas	Setup	Δt	Target	Target distance	Flow rate	Other	Δt_D
He	A	30, 35, 40	Conductor	24 mm	2 L/min	-	50 ns
	B	30, 35, 40	Conductor	32 mm	2 L/min	-	20 ns
	C	30, 35, 40	Insulator	24 mm	2 L/min	-	20 ns
	D	30, 35, 40	-	-	2 L/min	-	20 ns
	E	35	-	-	2 L/min	Ground ring	20 ns
	F	35	-	-	1 L/min	-	20 ns
	G	35	-	-	3 L/min	-	20 ns
	H	35	-	-	4 L/min	-	20 ns
Ne	A	20, 25, 30	Conductor	24 mm	2 L/min	-	50 ns
	B	20, 25, 30	Conductor	32 mm	2 L/min	-	50 ns
	C	20, 25, 30	Insulator	24 mm	2 L/min	-	50 ns
	D	20, 25, 30	-	-	2 L/min	-	50 ns
	E	30	-	-	2 L/min	Ground ring	50 ns
Ar	A	35	-	-	2 L/min	Ground ring	50 ns
	B	35	-	32 mm	2 L/min	-	20 ns
	C	35	-	-	2 L/min	Floating ring	50 ns
	D	35	Conductor	20 mm	2 L/min	Ground ring	50 ns
	E	35	Conductor	20 mm	2 L/min	-	50 ns
	F	35	-	-	2 L/min	-	50 ns
	G	35	Conductor	32 mm	2 L/min	-	50 ns

Table 2.1: Description of measure setups.

2.2 Neon flow

2.3 Helium flow

2.4 Argon flow

Chapter 3

Spectral Analysis

A fundamental aspect of the Plasma Coagulation Controller is what species are produced and deposited during its application. Various studies observed the spectrum of plasma DBD discharge in air at atmosferic pressure and ambient temperature ([9], [11]), meanly it presents peaks relative to reactive species from water, oxygen, nitrogen and its oxides at visible wavelenght, from 200 to 880 nm.

We are intersted in plasma that contains molecules involved in blood coagulation mechanisms, Reactive Oxidant Species (such as hydroxil radical OH) and Reactive Nitrogen Species (derived from nitric oxide NO) ([22]). In this spectroscopy study is given particular attention to them and their precursor, i.e. the presence of transitions relative to hydroxil, oxygen and molecular nitrogen.

3.1 Radiation emission

As remembered in previous chapters, at the exit of source head is produced plasma from a mixture gas of helium (or argon) and air, so along free electrons, there are ions and species that colliding with them are in an excited state, metastable or with small lifetime. All those reactive species partecipe in different reactions, and also in excitation and de-excitation reactions with conseguent emission of radiation. When an electron goes from state p at higher energy to state k of lower energy, is emitted radiation with central wavelenght λ_0. Power emitted by this radiation is given by radiant flux $d\phi_\lambda$ and selecting a solid angle as in figure, is possible to define radiance L_λ, and intensity I, as in equations 3.1. Intensity for a radiation ultimately depends on $n(p)$, population density for state p, and Einstein Coefficient for the transition A_{pk} that is typical for the transition ([3]).

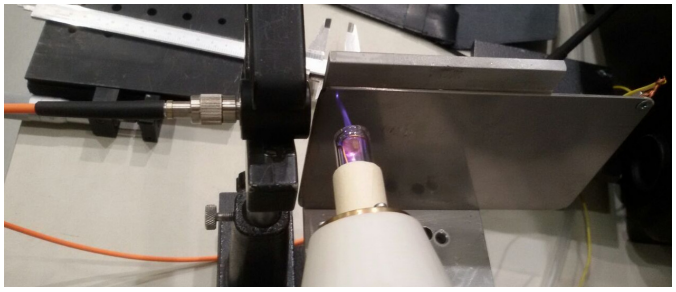

Figure 3.1: Setup of the experiment: there is the working source, the metal target and the optical setup on the left.

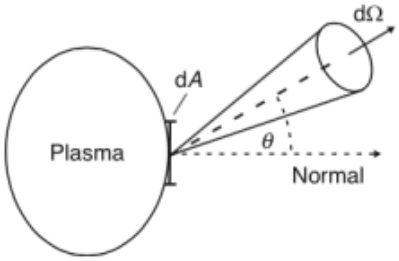

$$\lambda_0 = \frac{hc}{E_p - E_k}$$
$$L_\lambda = \frac{d^2\phi_\lambda}{dA\cos(\theta)d\Omega} \tag{3.1}$$
$$I = \int L_\lambda d\lambda = n(p)A_{pk}$$

Using air as gas, composed by molecules, at visible wavelenght are observed vibronic transitions where molecule goes from a vibrational state to another, with a change of vibrational quantum number ν, and/or from a rotational state to another, with change of quantum number J ([13], [36]). When there is a vibrational transition, each line corresponds to different numbers $\nu'-\nu''$, these are transitions well spaced in the spectrum, easy to recognize. Rotational transitions gives birth to bands of little-spaced peaks hard to resolve whitout an efficient spectrometer.

There are many reactions involving oxygen and nitrogen (see for example [20]), in this study we determine only principal transition observable with our spectrometer, to know dominant reactive species present in our plasma plume.

3.2 Experimental setup

For the source it's used a prototype that presents electrical specifics and settings same as source A described in previous chapters. A metal plate is positioned as target at a distance of 10 mm from plasma exit. To ignite plasma is used helium, with flow set to 2 L/min. To measure emission it's used a spectrometer IsoPlane, that thanks to diffraction separates emissions with different wavelenghts using a plane grating. The spectrometer has a focal lenght of 320 mm and is equipped with three different gratings: 150, 1200 and 2400 gg/mm, corresponding to different resolutions. As in figure 3.1, light emitted by plasma is collected with a quartz lens and passes trough an optical fiber connected to the spectrometer entry, while at the spectrometer exit there is a CCD camera of 2048 pixels and a count limit of 65 000.

Once a grating is chosen, the acquisition system can be set at a starting wavelenght and from there it takes measures until the end of the CCD, so for a different wavelenght interval for different gratings. For every measure is selected an appropriate acquisition time that permits to observe peaks with a good count number and avoid saturation.

It's important to stress out that, with this measuring method and due to complexity of plasma reactions and composition, it's not possible to extrapolate quantitative considerations between different species concentration. However it's possible to recognize the presence of certain species and make some considerations watching spectra variation with different experimental setup.

An intersting parameter is the working distance between source's head and target, so we observe spectra focalizing the lens in two different positions:

- position 1: as close as possible to plasma exit point
- position 2: close to the target, at 10 mm from plasma exit point

Reactions that produce and recombine reactive species, and consequently density and lifetime of species, are influenced by electric field and duration of the discharge. We observe spectra changing amplitude and frequency of the pulse, with tree different combinations that corresponds to different power coupled with the discharge:

- low: $f = 5\,\text{kHz}$ and $\Delta t = 15\,\mu\text{s}$
- medium: $f = 10\,\text{kHz}$ and $\Delta t = 10\,\mu\text{s}$
- high : $f = 15\,\text{kHz}$ and $\Delta t = 10\,\mu\text{s}$

3.3 Line recognition

To see what's generally produced in a discharge is taken a spectrum for the entire wavelenght's region intersted, from 230 to 800 nm, with standard setup of medium power and position 1. First is made a rapid acquisition with the lowest resolution possible, to see intersting regions and have an idea of required exposition times. After that is made a slow acquisition with higher resolution for all wavelenghts. The entire spectrum is reconstructed attaching different spectra, showed in figure 3.2, where are labelled principal transitions. For every measure is taken also a background spectrum, without plasma, to recognize peaks that are not from the plasma.

Data is read with IDL routines ([12]) and analyzed with ROOT TSpectrum.h library ([25]). Every spectrum is divided by its exposition time, to normalize different measures. Then is estimated the white noise contribution as mean value from a portion of the spectrum that doesn't presents peaks and its subtracted to the counts for each wavelenght. Peaks are then found with TSpectrum functions (where is possible to set a treshold in heigth and the general width for lines to be searched) and peaks from background are isolated in plasma spectra. Definitive position for each transition is found with a gaussian fit in an interval that takes into consideration the asymmetry where it's needed.

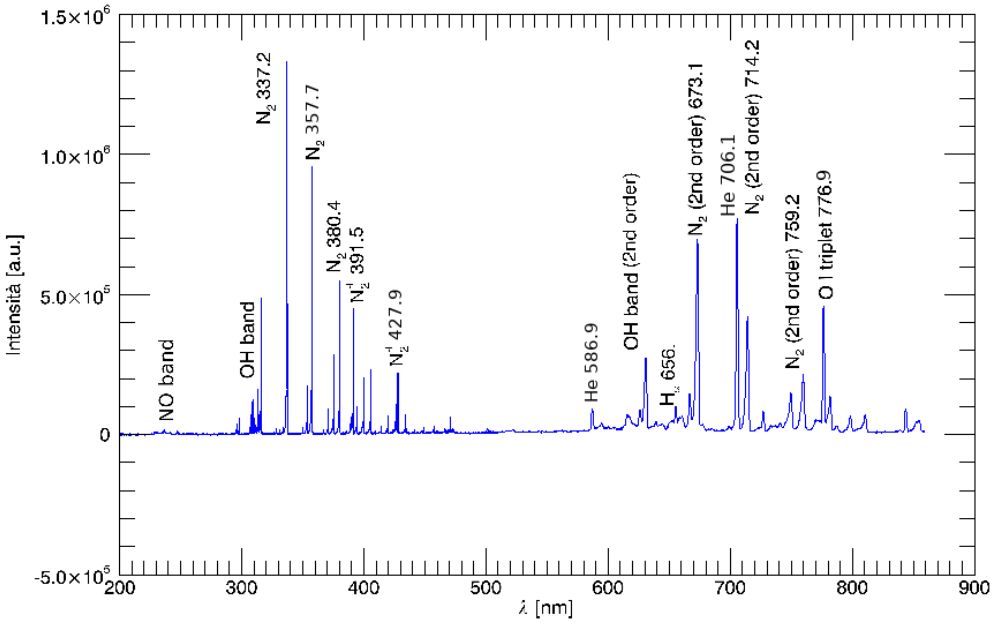

Figure 3.2: Spectrum with an helium flow of 2 L/min, pulse parameters of $f = 5\,\text{kHz}$ and $\Delta t = 16\,\mu\text{s}$, optical position 1, near plasma exit

As said before, this study is focused on measure related to ROS and NRS, so in lines for NO, OH and N_2.

NO lines Are observed two doublets for the transition $A^2\Sigma^+ \rightarrow X^2\Pi$ with vibrational numbers (0-0) and (0-1) ([18], [31]), presented in table 3.1. Intensities for the peaks are normalized with maximum value of 1000 for the acquisition, the table shows as the intensities for this transition is very low. Other transition relative to this molecule have even lower relative intensity and are not observed in our study.

λ [nm]	I [arb.u.]
236.31 ± 0.24	27
237.00 ± 0.15	26
247.02 ± 0.05	28
247.86 ± 0.12	27

Table 3.1: Peaks measured for NO.

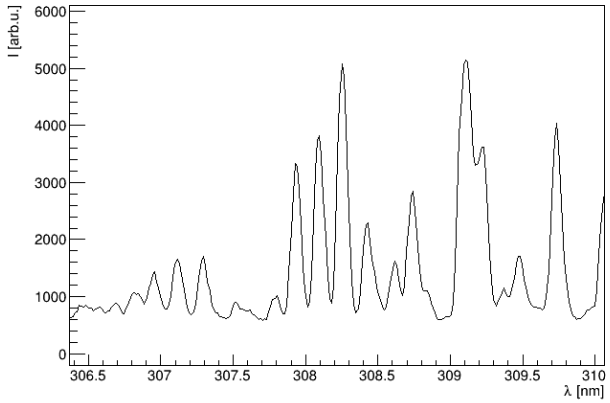

Figure 3.3: Zoom for OH peaks

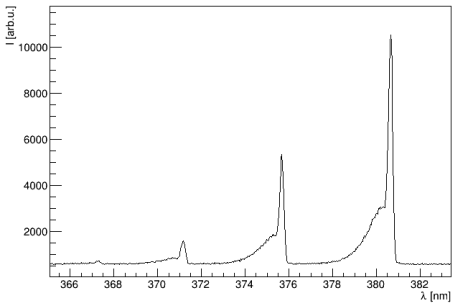

(a) Transitions with $\Delta\nu = 2$

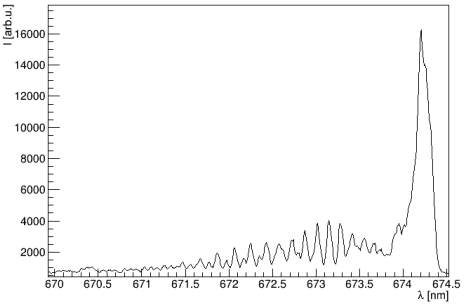

(b) Strongest line (0-0), 2^{nd} diffraction order

Figure 3.4: Zoom for N_2 transitions.

OH lines Is found the rotational band for transition ($A^2\Sigma$, $\nu' = 0 \rightarrow X^2\Pi$, $\nu'' = 0$), observing 13 principal lines ([14]). In figure 3.3 a zoom on the spectrum, in table 3.2 peak values.

N_2 and N_2^+ lines Measured spectrum presents several lines, including the strongest, for diatomic molecule dinitrogen. Is observed the Second Positive System for N_2 transition $C^3\Pi \rightarrow B^3\Pi$ and the First Negative System for N_2^+ transition $B^2\Sigma \rightarrow X^2\Sigma$, in table 3.3 peak values ([4], [6]). For N_2 is found also a band of multiple rotational lines centered around 336.58 ± 0.01 nm. Some of the peaks are seen in the second diffraction order, where there is more distance between lines. In figure 3.4 are presented two zooms for N_2 lines.

Atomic lines Are observed other lines from elements present in the plume ([21]):

- $\mathbf{H}_\alpha$ line corresponding to transition from quantum number $n = 3$ to $n = 2$

λ [nm]	I [arb.u.]
306.96 ± 0.01	53
307.11 ± 0.01	58
307.29 ± 0.01	62
307.94 ± 0.01	142
308.09 ± 0.01	148
308.26 ± 0.01	161
308.43 ± 0.01	112
308.62 ± 0.01	46
308.74 ± 0.01	137
309.11 ± 0.01	151
309.22 ± 0.01	120
309.45 ± 0.01	36
309.73 ± 0.01	125

Table 3.2: Peaks measured for OH.

	λ [nm]	I [arb.u.]	$(\nu' - \nu'')$
N_2	316.03 ± 0.01	381	(1-0)
	337.11 ± 0.01	1000	(0-0)
	357.77 ± 0.01	722	(0-1)
N_2	367.22 ± 0.20	58	(3-5)
	371.12 ± 0.04	172	(2-4)
	375.66 ± 0.02	232	(1-3)
	380.64 ± 0.02	423	(0-2)
N_2^+	391.50 ± 0.02	355	(0-0)
	427.45 ± 0.02	180	(0-1)

Table 3.3: Peaks measured for N_2 and N_2^+.

	λ [nm]	I [arb.u.]
H_α	655.96 ± 0.04	113
He	586.94 ± 0.05	122
	705.56 ± 0.01	649
O	776.89 ± 0.01	393

Table 3.4: Main peaks measured for other species found in plasma.

- **He** two of the strongest lines for helium
- **O** strong line of oxygen

3.4 Relative intensities

From comparision of spectra with different discharge parameters and different position for light collection point, is possible to extrapolate some informations on production rates of excited species.

Intensities are evaluated for OH and N_2 species, collectively for the lines in a wavelength range specific for the peaks. For OH lines is considered all the rotational band between 306-309 nm, lines for N_2 are separated in those between 335-337 nm (rotational band and (0-0) transition) and those between 368-382 nm (vibrational transitions with $\Delta\nu = 2$).

3.4.1 Pulse settings

Pulse settings characterize the discharge. As seen in chapter 1 for different frequencies we have near the same electric behavior, but it could influence specie's production rates. OH lines for both positions have same intensity with low and medium power setup, while is lower with higher frequency, with similar behavior in both positions. N_2 intensities also decrease with higher frequencies, for every lines, it reaches around 0.6% for $f = 15$ kHz in position 1, and lower values for position 2. It seems that production of those reactive species have rates dependant from pulse frequency, for high frequency there might be more relevant competitor reactions.

3.4.2 Line of sight

Positioning the line of sight of the spectrometer at different heigths along the plume axis, we can extrapolate informations about the lifetime of the species and the distance that they can travel. At 10 mm from the source, in position 2, intensities for OH decreases drastically, under 0.1% of values in position 1. OH species seems to have small lifetime or mobility, so deposition of this species is higher when closer to the target. For N_2

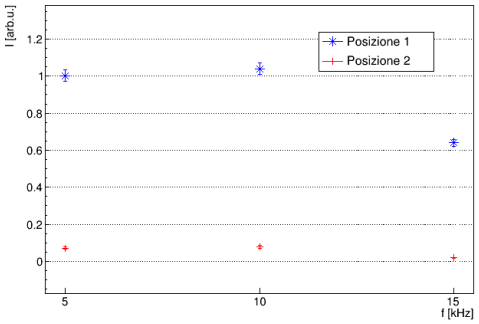

(a) OH intensities in range 306-309 nm

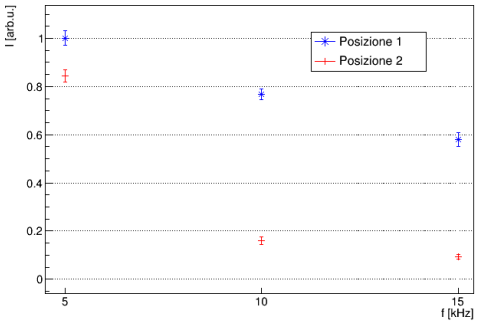

(b) N_2 intensities range 335-337 nm

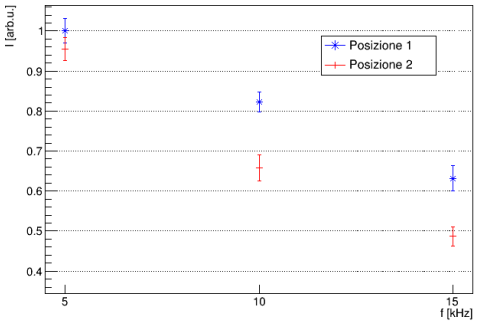

(c) N_2 intensities range 368-382 nm

Figure 3.5: Relative intensities in selected portions of the spectrum, for different frequencies, in blue for position 1 in red for position 2.

intensities are equal at low frequency for both positions, while for higher frequencies they decrease more for position 2. For low frequency, concentration of excited N_2 is high so even distant from the target we have high radiation emission. When it decreases, for higher frequencies, concentration lowers and we have few molecules that reach the target.

3.5 Estimation of plasma temperatures

From diatomic molecule's spectra it's possible to evaluate some parameters that are indicators of plasma's state: rotational temperatures for OH and N_2, T_r, and vibrational temperature for N_2, T_v. These parameters are estimation of the temperature at which thermal energy is comparable to the gap energy between rotational or vibrational state transitions, they can be defined as in equations 3.2 where ν is the vibrational quantum

number and I is the quantizied moment of inertia of the molecule.

$$\begin{aligned} T_r &= \frac{\hbar^2}{2k_B I} \\ T_v &= \frac{h\nu}{k_B} \end{aligned} \tag{3.2}$$

Rotational temperatures can be considered an estimation of neutral gas kinetic temperature, assuming that the population origins only from heavy particle collisions. Vibrational temperature gives an idea of the population of vibrational states, useful to determine chemical reactions inside plasma.

3.5.1 Rotational temperature for OH and for N_2

In rotational bands the intensity of a transition for a specific wavelength is proportional to the number density popolation of upper state (equation 3.1), that, considering a Maxwell-Boltzmann distribution, is proportional to the temperature of the species. In equation 3.3 the proportionality is explicitated, with D_0 parameter that depends on number of initial molecules, partition function of the rotational state and quantum rotational numbers for upper and lower state, S is the oscillator strenght specific for the molecule and E_r depends from a constant defined by the vibrational state and from quantum rotational number for upper state ([26]).

$$I = \left(\frac{2\pi}{\lambda}\right)^4 D_0 S \exp\left(-\frac{E_r}{k_B T_r}\right) \tag{3.3}$$

Given the high number of rotational lines, not distinguishable with our spectrometer, an approach to temperature estimation is to simulate spectra with different temperatures and to minimize differences for measured spectrum ([15]). In a predetermined range of temperatures we simulate different spectra with different temperatures, where each line is a gaussian peak with its width that takes into consideration broadning due to thermal motion, Doppler effect and measure resolution. For every spectrum is calculated the mean square differance, the temperature si selected as that associated with the minimum differance and are taken upper and lower limits where differance is larger by 5% of the minimum value. An example of the spectra is in figure 3.6, while resulting temperatures are in figure 3.7.

From estimated temperatures we can see that they are compatible with each other, for every distance and for every pulse setup. It's then possible to evaluate a mean value for the species, that are $T_{r,\mathrm{OH}} = 352 \pm 38\,\mathrm{K}$ and $T_{r,\mathrm{N_2}} = 321 \pm 41\,\mathrm{K}$, compatible with each other, and that, as said before, can be taken as an indicator of kinetic temperature for neutral species, so as temperature of the gas. This temperatures are a little higher then expected, but it can still be defined a cold plasma.

3.5.2 Vibrational temperature for N_2

Given a set of vibrational transition lines with defined $\Delta\nu = \nu' - \nu''$, their relative intensities are correlated to each other, with a proporionality that involves vibrational

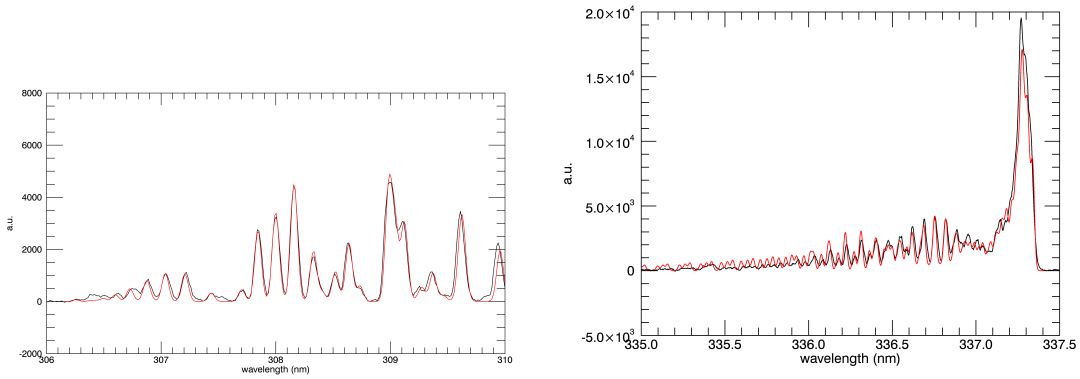

(a) OH **(b)** N_2

Figure 3.6: Example of optimal spectrum simulation for considered species.

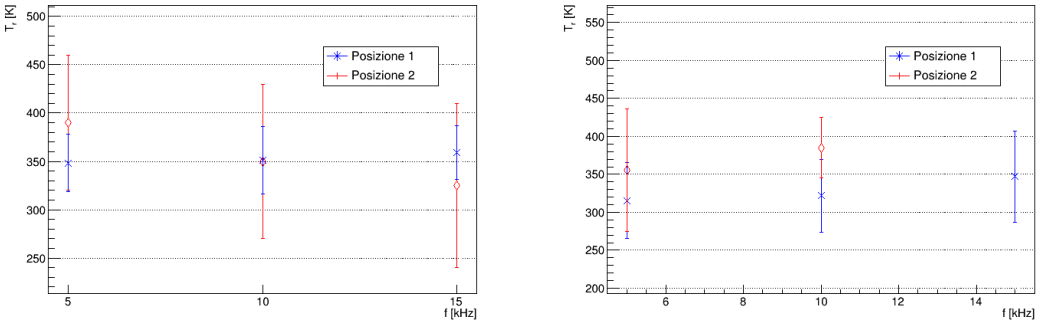

(a) OH **(b)** N_2

Figure 3.7: Estimation of rotational temperature of OH and N_2 molecules, for different frequencies, in blue position 1 in red position 2.

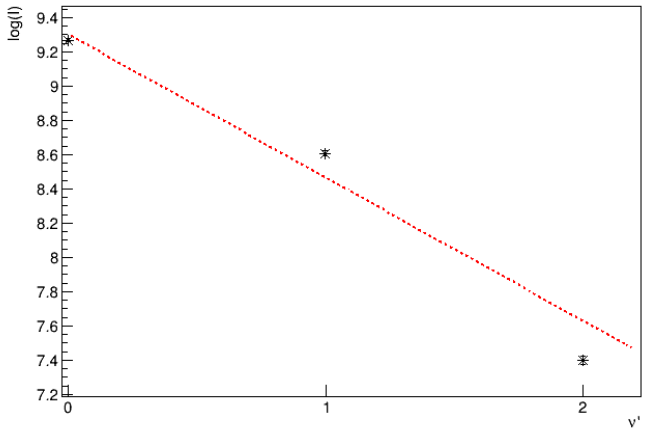

Figure 3.8: Example of a boltzmann graph for estimation of vibrational temperature, for low pulse setup and position 1.

temperature ([6]). Once estimated peak's intensities for considered transitions, it can be made the Boltzmann graph as in figure 3.8 and from then calculate T_v as in formula 3.4.

$$\begin{aligned} log(I(\nu') &= S\nu'' + I_0 \\ T_v[K] &= \frac{10^4}{3.57 \cdot S - 0.03} \end{aligned} \tag{3.4}$$

Results are presented in figure 3.9. For this parameter we have values compatible with each other at low and medium power pulse settings with a mean value of $T_v = 3405 \pm 154\,\mathrm{K}$, while we find a lower temperature for high power pulse settings $T_v = 2781 \pm 322\,\mathrm{K}$. It seems that whith an higher pulse frequency we have lower concentration of excited N_2 produced with lower mean energy.

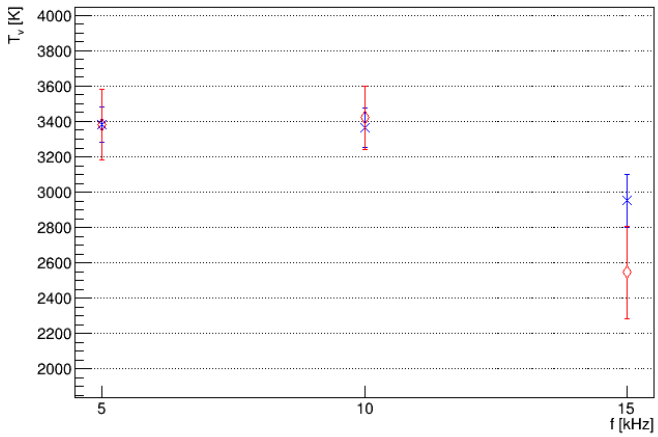

Figure 3.9: Estimation of vibrational temperature of N_2 molecule, for different frequencies, in blue position 1 in red position 2.

Bibliography

[1] URL: https://www.ptgrey.com/Content/Images/uploaded/Flea.pdf.

[2] URL: http://netpbm.sourceforge.net/doc/pgm.html.

[3] Hans-Joachim Kunze (auth.) *Introduction to Plasma Spectroscopy*. 1st ed. Springer Series on Atomic, Optical, and Plasma Physics 56. Springer-Verlag Berlin Heidelberg, 2009. ISBN: 9783642022326,3642022324.

[4] S. B. Bayram and M. V. Freamat. "Vibrational spectra of N2: An advanced undergraduate laboratory in atomic and molecular spectroscopy". In: *American Journal of Physics* 80.8 (2012), pp. 664–669. DOI: 10.1119/1.4722793. eprint: https://doi.org/10.1119/1.4722793. URL: https://doi.org/10.1119/1.4722793.

[5] D Breden, K Miki, and L L Raja. "Self-consistent two-dimensional modeling of cold atmospheric-pressure plasma jets/bullets". In: *Plasma Sources Science and Technology* 21.3 (2012), p. 034011. DOI: 10.1088/0963-0252/21/3/034011. URL: https://doi.org/10.1088%2F0963-0252%2F21%2F3%2F034011.

[6] N Britun et al. "Determination of the vibrational, rotational and electron temperatures in N2and Ar–N2rf discharge". In: *Journal of Physics D: Applied Physics* 40.4 (2007), pp. 1022–1029. DOI: 10.1088/0022-3727/40/4/016. URL: https://doi.org/10.1088%2F0022-3727%2F40%2F4%2F016.

[7] R. Brun. *ROOT documentation for Landau() function*. 1995. URL: https://root.cern.ch/doc/master/namespaceTMath.html#a656690875991a17d35e8a514f37f35d9.

[8] R. Brun. *ROOT documentation for TH2 class*. URL: https://root.cern.ch/doc/master/classTH2.html.

[9] Nisha Chandwani et al. "Determination of Rotational, Vibrational and Electron Temperatures in Dielectric Barrier Discharge in air at atmospheric pressure". In: (June 2014). DOI: 10.13140/RG.2.1.2078.6725.

[10] T Darny et al. "Analysis of conductive target influence in plasma jet experiments through helium metastable and electric field measurements". In: *Plasma Sources Science and Technology* 26.4 (2017), p. 045008. DOI: 10.1088/1361-6595/aa5b15. URL: https://doi.org/10.1088%2F1361-6595%2Faa5b15.

[11] Ioana Gerber et al. "Air Dielectric Barrier Discharge Plasma Source For In Vitro Cancer Studies". In: *Clinical Plasma Medicine* 9 (Feb. 2018), p. 4. DOI: 10.1016/j.cpme.2017.12.006.

[12] LIAM E. GUMLEY. *Practical IDL Programming*. San Francisco: Morgan Kaufmann, 2002. ISBN: 978-1-55860-700-2. DOI: https://doi.org/10.1016/B978-155860700-2.50003-3.

[13] Gerhard Herzberg. *Molecular Spectra and Molecular Structure I: Spectra of Diatomic Molecules*. 2nd. D. Van Nostrand, 1950. ISBN: 9780442033859,0442033850.

[14] C. de IZARRA. "COMPUTER SIMULATION OF THE UV OH BAND SPECTRUM". In: *International Journal of Modern Physics C* 11.05 (2000), pp. 987–998. DOI: 10.1142/S0129183100000857. eprint: https://doi.org/10.1142/S0129183100000857. URL: https://doi.org/10.1142/S0129183100000857.

[15] Charles de Izarra. "UV OH spectrum used as a molecular pyrometer". In: *Journal of Physics D: Applied Physics* 33.14 (2000), pp. 1697–1704. DOI: 10.1088/0022-3727/33/14/309. URL: https://doi.org/10.1088%2F0022-3727%2F33%2F14%2F309.

[16] Julien Jarrige, Mounir Laroussi, and Erdinc Karakas. "Formation and dynamics of plasma bullets in a non-thermal plasma jet: influence of the high-voltage parameters on the plume characteristics". In: *Plasma Sources Science and Technology* 19.6 (2010), p. 065005. DOI: 10.1088/0963-0252/19/6/065005. URL: https://doi.org/10.1088%2F0963-0252%2F19%2F6%2F065005.

[17] Julien Jarrige, Mounir Laroussi, and Erdinc Karakas. "Formation and dynamics of plasma bullets in a non-thermal plasma jet: influence of the high-voltage parameters on the plume characteristics". In: *Plasma Sources Science and Technology* 19.6 (2010), p. 065005. DOI: 10.1088/0963-0252/19/6/065005. URL: https://doi.org/10.1088%2F0963-0252%2F19%2F6%2F065005.

[18] Andre Knie. "Photon induced inner-shell excitation processes of nitrous oxide probed by angle resolved fluorescence and Auger-Electron spectrometry". Dr. Kassel: Univ. Kassel, 2013. ISBN: 978-3862194582.

[19] U. Kogelschatz, B. Eliasson, and W. Egli. "Dielectric-Barrier Discharges. Principle and Applications". In: *Journal de Physique IV Colloque* 07.C4 (1997), pp. C4–47–C4–66. DOI: 10.1051/jp4:1997405. URL: https://hal.archives-ouvertes.fr/jpa-00255561.

[20] I A Kossyi et al. "Kinetic scheme of the non-equilibrium discharge in nitrogen-oxygen mixtures". In: *Plasma Sources Science and Technology* 1.3 (1992), pp. 207–220. DOI: 10.1088/0963-0252/1/3/011. URL: https://doi.org/10.1088%2F0963-0252%2F1%2F3%2F011.

[21] A. Kramida et al. 2018.

[22] S. P. Kuo et al. "Applications of Air Plasma for Wound Bleeding Control and Healing". In: *IEEE Transactions on Plasma Science* 40.4 (2012), pp. 1117–1123. ISSN: 0093-3813. DOI: 10.1109/TPS.2012.2184142.

[23] M.A. Lieberman and A.J. Lichtenberg. *Principles of Plasma Discharges and Materials Processing*. Wiley, 1994. ISBN: 9780471005773. URL: https://books.google.it/books?id=-cloQgAACAAJ.

[24] N Mericam-Bourdet et al. "Experimental investigations of plasma bullets". In: *Journal of Physics D: Applied Physics* 42.5 (2009), p. 055207. DOI: 10.1088/0022-3727/42/5/055207. URL: https://doi.org/10.1088%2F0022-3727%2F42%2F5%2F055207.

[25] M. Miroslav. *ROOT documentation for TSpectrum class.* URL: https://root.cern.ch/doc/v614/classTSpectrum.html.

[26] Se Youn Moon and W. Choe. "A comparative study of rotational temperatures using diatomic OH, O2 and N2+ molecular spectra emitted from atmospheric plasmas". In: *Spectrochimica Acta Part B: Atomic Spectroscopy* 58.2 (2003). INTERSIBGEOCHEM 01, pp. 249 –257. ISSN: 0584-8547. DOI: https://doi.org/10.1016/S0584-8547(02)00259-8. URL: http://www.sciencedirect.com/science/article/pii/S0584854702002598.

[27] Seth A. Norberg, Eric Johnsen, and Mark J. Kushner. "Helium atmospheric pressure plasma jets touching dielectric and metal surfaces". In: *Journal of Applied Physics* 118.1 (2015), p. 013301. DOI: 10.1063/1.4923345.

[28] Cecilia Piferi. "Caratterizzazione di sorgenti di plasma per applicazioni biomediche". 2016/17.

[29] Eric Robert et al. "Experimental Study of a Compact Nanosecond Plasma Gun". In: *Plasma Processes and Polymers* 6.12 (2009), pp. 795–802. DOI: 10.1002/ppap.200900078.

[30] *ROOT documentation for TVirtualFFT class.* URL: https://root.cern.ch/doc/master/classTVirtualFFT.html.

[31] H.A. Van Sprang, H.H. Brongersma, and F.J. De Heer. "Absolute emission cross sections for the calibration of optical detection systems in the 120–250 nm range". In: *Chemical Physics Letters* 65.1 (1979), pp. 55 –60. ISSN: 0009-2614. DOI: https://doi.org/10.1016/0009-2614(79)80124-4. URL: http://www.sciencedirect.com/science/article/pii/0009261479801244.

[32] Takaaki Tomai, Tsuyohito Ito, and Kazuo Terashima. "Generation of dielectric barrier discharge in high-pressure N2 and CO2 environments up to supercritical conditions". In: *Thin Solid Films* 506-507 (2006). The Joint Meeting of 7th APCPST (Asia Pacific Conference on Plasma Science and Technology) and 17th SPSM (Symposium on Plasma Science for Materials), pp. 409 –413. ISSN: 0040-6090. DOI: https://doi.org/10.1016/j.tsf.2005.08.101. URL: http://www.sciencedirect.com/science/article/pii/S0040609005013052.

[33] Lewi Tonks and Irving Langmuir. "A General Theory of the Plasma of an Arc". In: *Phys. Rev.* 34 (6 1929), pp. 876–922. DOI: 10.1103/PhysRev.34.876. URL: https://link.aps.org/doi/10.1103/PhysRev.34.876.

[34] Stephanie Tümmel et al. “Low Temperature Plasma Treatment of Living Human Cells”. In: *Plasma Processes and Polymers* 4.S1 (2007), S465–S469. DOI: 10.1002/ppap.200731208. eprint: https://onlinelibrary.wiley.com/doi/pdf/10.1002/ppap.200731208. URL: https://onlinelibrary.wiley.com/doi/abs/10.1002/ppap.200731208.

[35] J. Upadhyay et al. “Development of high-voltage pulse generator with variable amplitude and duration”. In: *Review of Scientific Instruments* 85.6 (2014), p. 064704. DOI: 10.1063/1.4884883.

[36] Wikipedia contributors. *Vibronic spectroscopy*. 2018. URL: https://en.wikipedia.org/w/index.php?title=Vibronic_spectroscopy&oldid=823782704.

[37] Wen Yan and Demetre J. Economou. “Simulation of a non-equilibrium helium plasma bullet emerging into oxygen at high pressure (250–760Torr) and interacting with a substrate”. In: *Journal of Applied Physics* 120.12 (2016), p. 123304. DOI: 10.1063/1.4963115.